



Resistive switching in silicon suboxide films

Adnan Mehonic, Sébastien Cueff, Maciej Wojdak, Stephen Hudziak, Olivier Jambois et al.

Citation: *J. Appl. Phys.* **111**, 074507 (2012); doi: 10.1063/1.3701581

View online: <http://dx.doi.org/10.1063/1.3701581>

View Table of Contents: <http://jap.aip.org/resource/1/JAPIAU/v111/i7>

Published by the [American Institute of Physics](#).

Related Articles

Electrostatic force between two conducting spheres at constant potential difference
J. Appl. Phys. **111**, 076102 (2012)

Second and higher harmonics generation with memristive systems
Appl. Phys. Lett. **100**, 133109 (2012)

Engineering nonlinearity into memristors for passive crossbar applications
Appl. Phys. Lett. **100**, 113501 (2012)

A novel method of temperature compensation for piezoresistive microcantilever-based sensors
Rev. Sci. Instrum. **83**, 035002 (2012)

Non-volatile gated variable resistor based on doped $\text{La}_2\text{CuO}_{4+\delta}$ and SrTiO_3 heterostructures
J. Appl. Phys. **111**, 056101 (2012)

Additional information on *J. Appl. Phys.*

Journal Homepage: <http://jap.aip.org/>

Journal Information: http://jap.aip.org/about/about_the_journal

Top downloads: http://jap.aip.org/features/most_downloaded

Information for Authors: <http://jap.aip.org/authors>

ADVERTISEMENT



FIND THE NEEDLE IN THE HIRING HAYSTACK

Post jobs and reach
thousands of hard-to-find
scientists with specific skills



<http://careers.physicstoday.org/post.cfm>

physicstoday JOBS

Resistive switching in silicon suboxide films

Adnan Mehonic,^{1,a)} Sébastien Cueff,² Maciej Wojdak,¹ Stephen Hudziak,¹ Olivier Jambois,³ Christophe Labbé,² Blas Garrido,³ Richard Rizk,² and Anthony J. Kenyon^{1,b)}

¹Department of Electronic & Electrical Engineering, UCL, Torrington Place, London WC1E 7JE, United Kingdom

²CIMAP, UMR CNRS 6252 ENSICAEN, 6 Boulevard Maréchal Juin, 14050 Caen Cedex 4, France

³MIND-IN2UB, Department Electrònica, Universitat de Barcelona, Martí i Franquès 1, 08028, Barcelona, CAT, Spain

(Received 16 December 2011; accepted 27 February 2012; published online 6 April 2012)

We report a study of resistive switching in a silicon-based memristor/resistive RAM (RRAM) device in which the active layer is silicon-rich silica. The resistive switching phenomenon is an intrinsic property of the silicon-rich oxide layer and does not depend on the diffusion of metallic ions to form conductive paths. In contrast to other work in the literature, switching occurs in ambient conditions, and is not limited to the surface of the active material. We propose a switching mechanism driven by competing field-driven formation and current-driven destruction of filamentary conductive pathways. We demonstrate that conduction is dominated by trap assisted tunneling through noncontinuous conduction paths consisting of silicon nanoinclusions in a highly nonstoichiometric suboxide phase. We hypothesize that such nanoinclusions nucleate preferentially at internal grain boundaries in nanostructured films. Switching exhibits the pinched hysteresis I/V loop characteristic of memristive systems, and on/off resistance ratios of 10^4 :1 or higher can be easily achieved. Scanning tunneling microscopy suggests that switchable conductive pathways are 10 nm in diameter or smaller. Programming currents can be as low as 2 μA , and transition times are on the nanosecond scale. © 2012 American Institute of Physics.

[<http://dx.doi.org/10.1063/1.3701581>]

I. INTRODUCTION

Nonvolatile memories based on resistive switching have recently attracted significant attention.¹ In particular, the two-terminal elements known as memristors² offer a potential solution to the problem of decreased controllability of charge in semiconductor memories as devices scale to ever-smaller dimensions. First postulated by Leon Chua in 1971 as the “missing” fourth passive circuit element,² the first practical realization of the memristor, in titanium dioxide, was not reported until 2008.³ Such devices have a wide range of potential applications in high-density memories, novel processor architectures, and neural networks. Consequently, the development of a practical CMOS device is a very attractive prospect for integration with current silicon technologies. Proof-of-principle memory systems exploiting memristors have already been demonstrated,^{1,3–7} typically consisting of multilayer structures in which conductive pathways form under the application of external fields. Titanium dioxide multilayers, exploiting field-driven redistribution of oxygen ions, were the first reported memristor devices,³ but there have also been promising reports of silicon-based resistive switches.^{4,8} In the latter case, two approaches have been successful: field-driven diffusion of silver ions from metal contacts into amorphous silicon layers^{5,8} and switchable conductive pathways on the surface of silicon-rich silica (SiO_x) pillars.⁴ However, in CMOS processing the diffusion of metallic ions is undesir-

able, as this could potentially endanger the operation of surrounding electronics. The intrinsic resistive switching of silicon oxide is a more appealing mechanism. The first such system was demonstrated by Yao *et al.*,⁴ who reported a switchable silicon conductive path formed on the vertical surface of a silicon-rich silica pillar. However, the operation of such a device is possible only under vacuum due to oxidation of silicon conductive pathways on the device surface under ambient conditions. The authors reported no evidence of high-contrast controllable resistive switching in continuous films of silicon oxide: instead, silicon nanofilaments at vertical surfaces of mesa structures were proposed as the switching elements. In contrast, we demonstrate here a device operating under ambient conditions that relies on switching within a continuous thin film of silicon-rich silica. The device can be cycled between high resistance “OFF” and low resistance “ON” states with a resistance contrast of 10,000 or more. Both states are stable, persisting for at least 120 h, and likely much longer.

II. EXPERIMENTAL DETAILS

Our test devices [Fig. 1(b)] contain thin (15–120 nm) SiO_x layers sandwiched between a p -type silicon wafer and n -type top electrodes (a range of electrode sizes was used— from 1.5 mm \times 4 mm to 125 μm \times 125 μm). To address thermal budget issues during fabrication, we investigated two configurations: one with n -type polycrystalline silicon top electrodes, requiring a 950 °C anneal to optimize conductivity, and a second with indium tin oxide (ITO) electrodes,

^{a)}Electronic mail: a.mehonic@ee.ucl.ac.uk.

^{b)}Electronic mail: t.kenyon@ee.ucl.ac.uk.

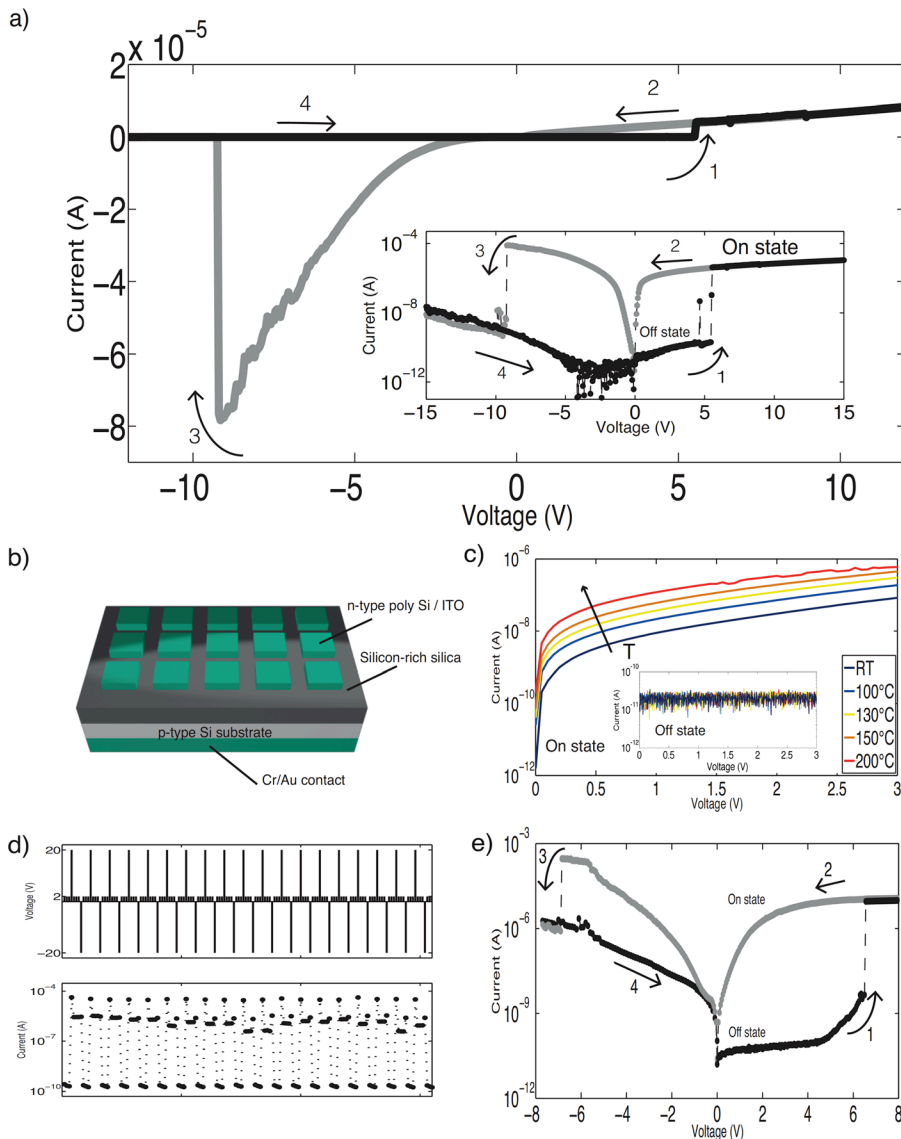


FIG. 1. (a) IV characteristics ($125 \mu\text{m} \times 125 \mu\text{m}$ top electrode). The black line in the positive bias shows a transition from OFF to ON state. The gray line shows a full ON state afterwards. The gray line in the negative bias shows a transition from ON to OFF state and the black line shows a full OFF state afterwards. Inset: Logarithmic representation. (b) Device schematic. (c) ON and OFF states dependence on increasing temperature. (d) Switching cycles using voltage pulses of +20, -20, and +2 V for setting, resetting and reading, respectively. (e) IV characteristics for device with poly-Si top contact (30 at. % excess Si, 37 nm thick layer, $125 \mu\text{m} \times 125 \mu\text{m}$ contact size).

deposited at room temperature. The former is readily integrated with front-end CMOS processes; the latter allows memristors to be integrated onto existing device layers without high temperature processing.

The SiO_x layers were deposited by magnetron co-sputtering onto *p*-type, B-doped silicon (100) wafers. Samples were deposited at 500°C . Two confocal cathodes were used: SiO_2 and Si, under a pure argon plasma. Layer thicknesses between 15 nm and 120 nm (measured by spectroscopic ellipsometry) were used for different devices, and excess silicon content was between 11 and 30 at. % for different samples (measured by XPS: Perkin-Elmer PHI-5500). Results reported here were from samples containing 11 at. % excess Si. Samples were annealed at 900°C or at 500°C post deposition in an argon atmosphere. The initial sample annealing temperature had little effect on the switching behavior of the devices.

For one batch of samples, 185 nm of *n*-type silicon (phosphorous doped, resistivity $10 \text{ m}\Omega\text{cm}$) was deposited on top of the SiO_x layer by low pressure chemical vapor deposition (LPCVD). After growth, samples were annealed at 950°C for 30 min in nitrogen to activate the dopants and

achieve a final resistivity of $1 \text{ m}\Omega\text{cm}$. After a buffered HF dip to remove surface oxide, 100 nm of chrome was sputtered onto the front side, photoresist spun on, and the sample exposed with a chrome-on-glass mask. The mask contained a number of different electrode sizes — from $1.5 \text{ mm} \times 4 \text{ mm}$ to $125 \mu\text{m} \times 125 \mu\text{m}$. The photoresist was developed, then the exposed chrome etched. Removal of the remaining photoresist was followed by a buffered HF etch and the samples were etched in TMAH, 25% solution at 60°C , for 40 s. Finally, the chrome was etched, and the samples rinsed and blow-dried in N_2 .

A second set had 70 nm thick ITO layers deposited by sputtering, followed by photolithographic contact definition using the same mask as for set 1. The ITO layer was etched using hydrochloric acid. Chrome-gold Ohmic contacts were provided on the back sides of all wafers by evaporation (10 nm Cr, followed by 100 nm Au).

An asymmetric structure (*n*-type top electrodes (*n*-Si or ITO); *p*-type substrate), allows us to define two regimes in our MOS structure. Applying a negative potential to the top electrode allows higher currents to flow (negative bias); a positive potential results in lower currents (positive bias). In

similar oxide based resistive systems, externally controlled current compliance has been required for successful operation. High current passing through thin oxide film could cause irreversible hard breakdown thus leading to device failure. An asymmetric design allows us to cycle the device without the need for external current compliance.

I/V and I/t measurements were performed using a Keithley 4200 Semiconductor Characterization System and a Signatone probe station. STM measurements were taken using a Nanosurf easyScan 2 scanning tunneling microscope. Atomic force microscopy (AFM) measurements were taken using a Veeco Dimension 3100 AFM operating in contact mode.

All experiments were performed in ambient conditions in an open laboratory. All shown results are performed on the devices with the top ITO contact, 37 nm thick active layer and 11 at. % excess Si unless otherwise specified.

III. RESULTS AND DISCUSSION

A. Current–voltage characteristics

Figure 1(a) shows typical I/V results (contact size: $125 \mu\text{m} \times 125 \mu\text{m}$). We should here note that, of the devices tested, 77% exhibited resistive switching as described. We have not performed any device or process optimization, and we are therefore confident that this figure can be significantly increased. The purpose of this report is to demonstrate proof-of-principle resistive switching in bulk SiO_x , and to probe the switching mechanism. Hysteresis is evident in Fig. 1(a) in both positive and negative bias, and the data show the pinched hysteresis curve characteristic of memristive systems. In positive bias, the initial high impedance (OFF) state

switches to a low impedance (ON) state at a threshold voltage (black line in the positive bias). This is the “set” process. Reducing the voltage below threshold does not switch the device to its initial state, and much larger currents flow (gray line). Resistance contrast between the two states is up to six orders of magnitude in devices studied to date; four orders are typical. Transitions between states are abrupt (i.e., faster than the sampling time of our measurement) and do not depend on voltage sweep speed. The results shown are obtained with an acquisition time of around 15 ms per point (the maximum resolution of our equipment), which is equivalent to a sweep rate of 3.33 Vs^{-1} with 300 points sampled. After switching, the device stays in the low impedance state until a negative bias is applied and certain critical current is reached. Although the low resistance to high resistance (“reset”) switching process can be achieved in both polarities, the negative bias is much more efficient as higher currents can be achieved with lower voltages than in positive bias. A sharp drop in current can be seen (gray line in negative bias) when the required current level is reached under negative bias. Note in the example shown in Fig. 1(a) that the device returns to the initial high resistance OFF state following the reset process—in some cases it is possible to return the device to a partially OFF state with an intermediate resistance [see Fig. 2(c)]. The formation (“set”) process can be achieved by again applying a positive bias.

Samples with silicon top contacts exhibited switching behavior that was qualitatively similar to those with ITO contacts [Fig. 1(e)], but higher reset currents were required, leading to reduced device endurance. We believe that this can be attributed to an additional annealing step at 950°C

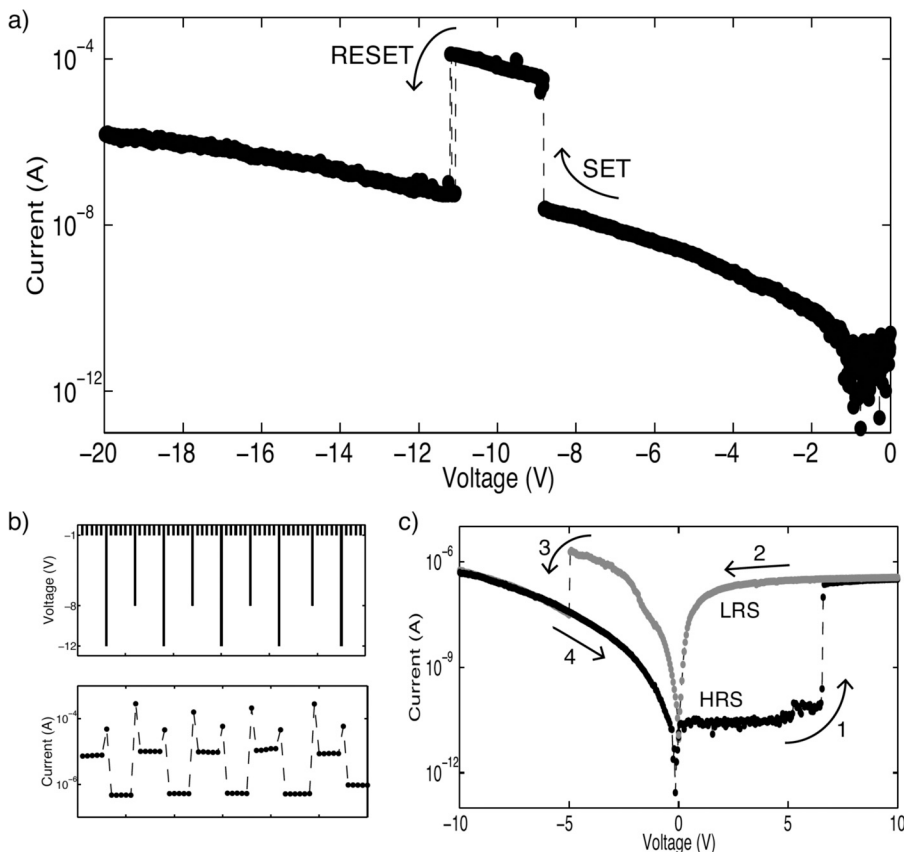


FIG. 2. (a) Unipolar switching for device with ITO contact ($250 \mu\text{m} \times 250 \mu\text{m}$ contact size) (b) Unipolar programming with -8 V (set), -12 V (reset), and -1 V (read), (c) IV characteristics ($125 \mu\text{m} \times 125 \mu\text{m}$ top electrode).

required to maximize the conductivity of the *n*-type poly-Si layer. This is likely to produce a high density of silicon nano-inclusions within the film as a result of phase separation, allowing strong conductive pathways to form. Future implementations of all-silicon memristors will therefore require careful control of the processing thermal budget. Further work on device and processing optimization is under way.

Set and reset voltages can vary from the values shown in Fig. 1(a), depending on the history of the devices (duration and magnitude of the last applied voltage bias). However, short voltage pulses of ± 15 V or greater almost always trigger switching in healthy devices. These switching processes are repeatable, and the states stable for at least 120 h at room temperature. Figure 1(d) illustrates sequential cycling between high and low resistance states (device programming). For the results shown in Fig. 1(d) a programmed sweep mode was used with a sweep speed of around 50 ms per point (the maximum resolution of our equipment in this mode). The applied voltages were: +20 V (set), -20 V (reset), and +2 V (read). In the best devices programming can be achieved using 10 V pulses as short as 90 ns (the limit of our equipment resolution — for these measurements a stand-alone pulse generator was used, rather than the Keithley 4200). Reset current in these devices can be up to 100 μ A [typical is around 10 μ A, and in the best devices this can be as low as 2 μ A (Fig. 2)], which is still sufficiently low for memory applications. The read operation uses approximately an order of magnitude less current in the ON state. The variations in reset current are likely an effect of non-homogeneous film deposition. Material optimization should provide better uniformity of reset currents and programming voltages.

Figure 1(c) shows conduction dependence on temperature in both ON and OFF state. The result shows typical semiconductor behavior (resistance decreases with increased temperature), suggesting no metallic conduction in the ON state. Temperature increase does not affect the OFF state.

The ON current does not show a clear tendency to scale with contact size (we tested this with the 3 contact sizes of $125 \mu\text{m} \times 125 \mu\text{m}$, $250 \mu\text{m} \times 250 \mu\text{m}$ and $500 \mu\text{m} \times 500 \mu\text{m}$), suggesting carrier transport via individual conductive pathways. Contrary to other reports, in which switching is attributed to ionic diffusion from metallic contacts,⁹ the switching in our device is an intrinsic property of the silicon-rich silica layer, so we hypothesize that the conductive pathways are

related to the excess silicon content. In addition, we note that indium tin oxide is known to be very good diffusion barrier,¹⁰ further supporting our conclusion that metallic diffusion is not the source of the resistive switching. Moreover, devices with poly-silicon contacts show very similar resistive switching behavior [Fig. 1(e)]. When devices are heated up to 200 °C during test, the conductivity in the ON state shows a reversible increase, confirming the nonmetallic nature of the conduction path [Fig. 1(c)]. As the current is determined by the conductive pathway rather than the availability of carriers from the substrate, we conclude that the pathways are silicon, rather than diffused metal ions from the ITO top contact, or from contamination of the active layer. Contrary to this, systems exhibiting metallic filament conduction show a decrease in the ON state conduction with increasing temperature due to filament melting.¹¹

Figure 2(a) demonstrates unipolar switching of the device under negative bias. Both set and reset processes can be seen, with reset occurring once the current has reached a critical value. The switching process is thus inherently unipolar. Figure 2(b) shows unipolar programming of a device, showing that it is possible to repeatedly set and reset the resistive states using one polarity of voltage pulse. We note, however, that only a small number of devices exhibited unipolar switching, which we ascribe to the asymmetric structure of our devices — we discuss this further in the discussion section below.

Figure 2(c) shows an IV curve for a sample with an ITO top contact in which the reset process puts the device into a partially OFF state; although the resistance is reduced by approximately one order of magnitude by the reset pulse, the device does not return to the initial fully OFF state. This suggests the possibility of multilevel operation of devices.

We note that the both ON read current and reset current could be increased if much larger contacts are used ($2 \text{ mm} \times 2 \text{ mm}$ or larger). In this case it is likely that a number of parallel conduction paths are formed. Further evidence of multilevel switching is shown in Fig. 3. In this case, three distinct levels, together with competing set/reset processes are shown in Figs. 3(a) and 3(b).

B. Current–time characteristics

Figures 4(a) and 4(b) show current–time graphs under constant voltage biases of -8 and -10 V for the $2 \text{ mm} \times 2 \text{ mm}$

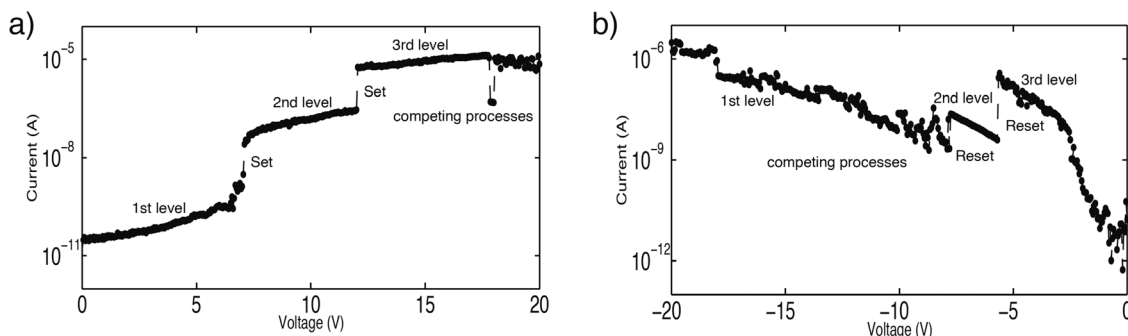


FIG. 3. (a) IV curve (in positive bias) shows three distinct levels (two set processes and competing process) (b) IV curve (in negative bias) shows three distinct levels (two reset processes and competing process).

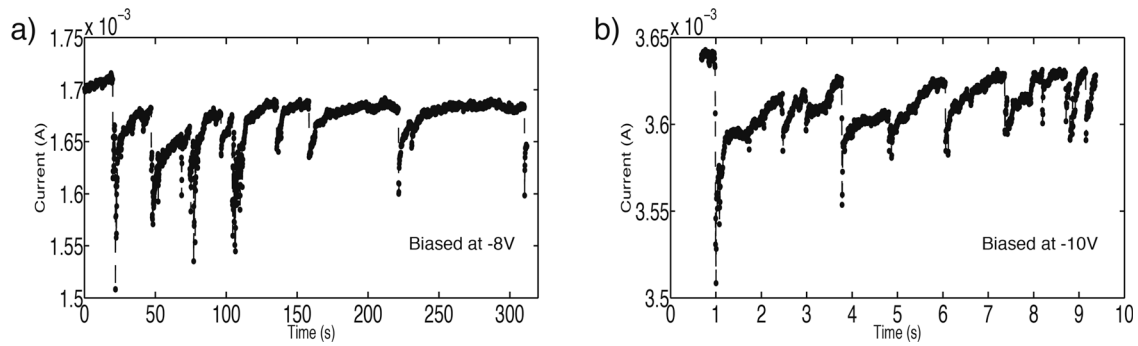


FIG. 4. Current-time graphs under a constant voltage bias of (a) -8 V and (b) -10 V.

contact: it is evident that formation (set) and destruction (reset) processes act in opposition. In the case of larger contacts, it is likely that multiple conduction paths are formed, resulting in increased reset negative voltage and current. Clear transitions between two states can be seen with rapid current drops (up to 10%) followed by slower, exponential, increases indicating multiple conduction paths where switching occurs in one or a few paths while other paths remains intact. Recovery speed is proportional to the applied voltage: the average time constant decreases from 10 to around 0.5 s on changing the bias from -8 to -10 V. Higher negative voltages reset the device without repetitive transitions to the ON state. However, the ON state is stable if the bias is lower than 6 V. We distinguish two conditions: high field and low current (positive bias) in which pathway formation is favored, and high field and high current (negative bias) in which destruction dominates. We therefore propose a switching mechanism based on competing field-driven formation and current-driven destruction of conductive pathways.

C. Impedance spectroscopy and conduction mechanism

Impedance spectroscopy^{1,12} reveals different conduction mechanisms in ON and OFF states, and is used to examine the nature of conducting path. In the OFF state, a single arc suggests an equivalent circuit model with a single parallel capacitor and resistor ($R = 2.81 \times 10^{10} \Omega$, $C = 2.61 \times 10^{-12}$ F). This high resistance is governed by the bulk properties of the SiO_x layer. However, in the ON state, two clear arcs are seen, suggesting additional parallel resistances and capacitances appearing in series. This is consistent both with formation and destruction of conductive pathways, and with previous studies of carrier transport in such films. The latter can be modeled as shown in the inset of Fig. 5(b) ($R_1 = 1.68 \times 10^6 \Omega$, $C_1 = 1.72 \times 10^{-10}$ F; $R_{eq} = 2.58 \times 10^6 \Omega$, C_{eq} (equivalent capacitance of series capacitors) = 3.03×10^{-10} F). The imaginary part of the impedance remains negative at frequencies between 1 and 10^7 Hz, suggesting no inductive behavior, which would be typical for metallic filaments.

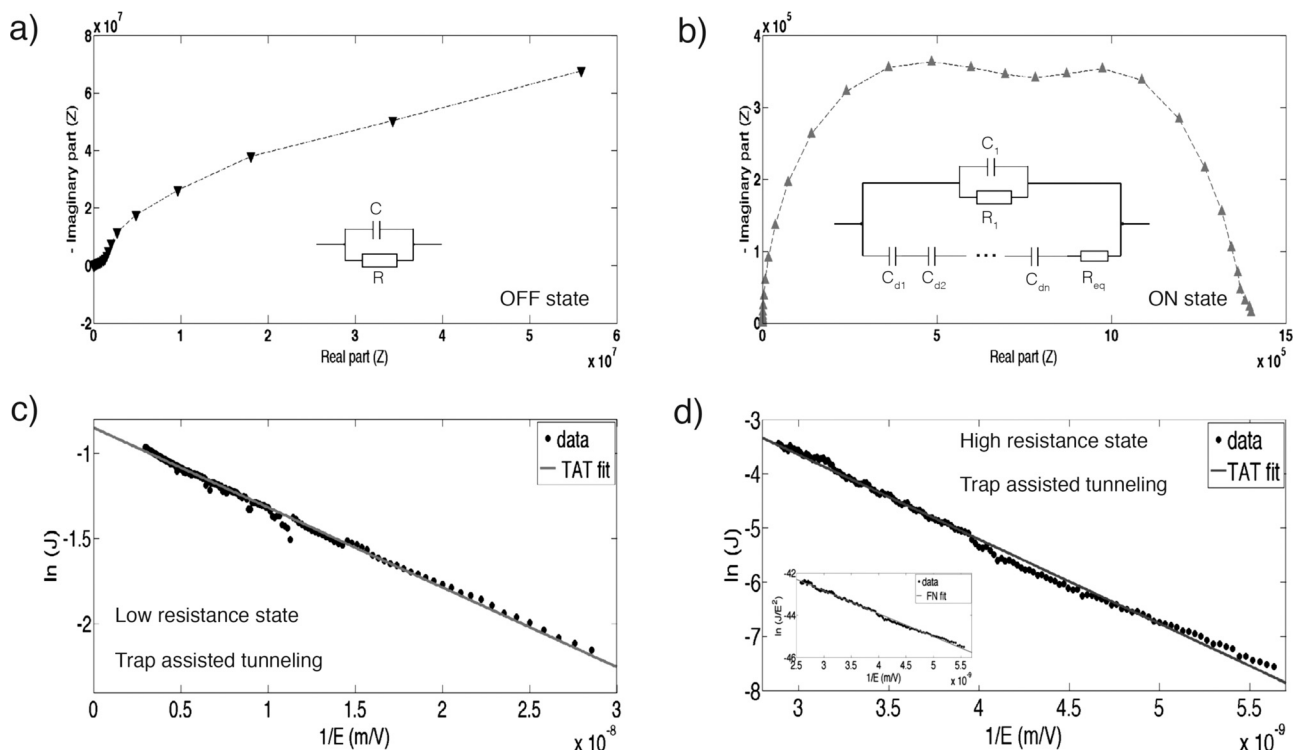


FIG. 5. Cole – Cole plots with equivalent circuits under 1 V in (a) OFF state and (b) ON state. Trap assisted tunneling fit in (c) ON (low resistance) state and (d) OFF (high resistance) state (Inset: Fowler-Nordheim tunneling fit in OFF state).

Trap-assisted tunneling dominates the conduction mechanism in both ON (low resistance) and partially OFF states (high resistance) (here, partially off refers to the black line in reverse bias in Fig. 2; in the fully OFF state, there is insufficient current to measure conduction). Figure 5(d) shows data fit in the partially OFF state with the trap assisted tunneling model. The obtained trap depth is 0.52 eV. A reasonably good fit (especially at higher fields) can also be achieved with the Fowler-Nordheim tunneling (F-N) model, as shown in the inset of Fig. 5(d). In this case, a barrier height of 0.66 eV is obtained which is consistent with literature results reported by DiMaria.¹³

ON state conduction is modeled best using trap assisted tunneling for all applied fields [Fig. 5(c)]. The obtained value for trap depth is 0.086 eV. In order to make sense of this result, we note that it is likely that the matrix in between the silicon nanoinclusions will be a suboxide of silicon with a much smaller bandgap than stoichiometric SiO₂, resulting in a much lower barrier height — intermediate between the band offset of the Si/SiO₂ interface, and zero. A chain of nanoparticles is formed, and transport proceeds via trap-assisted tunneling (TAT) between adjacent nanoparticles.^{14,15} The larger trap depth in the partially OFF state can be ascribed to a reduction in the stoichiometry of gaps in the conductive pathway following removal of nanoinclusions by Joule heating. The trap depth here increases, moving toward a value close to the Si/SiO₂ band offset. Note that we did not observe Fowler-Nordheim tunneling in devices in the fully ON state.

D. Scanning tunneling microscopy and atomic force microscopy

It is well established that films grown by sputtering often exhibit columnar or granular growth.¹⁶ Boundaries between adjacent columns can extend through the whole thickness of the film, effectively connecting the top and bottom of the active layer. Atomic force microscopy [Fig. 6(b)] of sample surfaces indicated periodic 5–10 nm high circular dome-shaped surface features that varied in diameter from 10 to 50 nm. STM of these structures showed high conductivity at the edges of the features, and low conductivity at the center [Fig. 6(c)]. Such pathways are around 5–30 nm in diameter, suggesting that devices may be scaled down to the nanometer dimensions to achieve very high levels of integration. Figure 6(a) shows I/V measurements of the two regions, highlighting the difference in conductivity. Figure 6(d) is a schematic of the film structure, showing columnar structures with silicon nanoinclusions nucleating at column boundaries. Such a structure is consistent with both AFM and STM results.

E. Switching model

In order to explain the memristive behavior of our devices, we first note that silicon-rich silica is a metastable material that readily segregates into silicon and silicon dioxide.^{17,18} It contains a high concentration of oxygen vacancies,¹⁹ which can be driven by high temperature annealing and consequent diffusion of vacancies and silicon to form silicon nanoclusters. In the

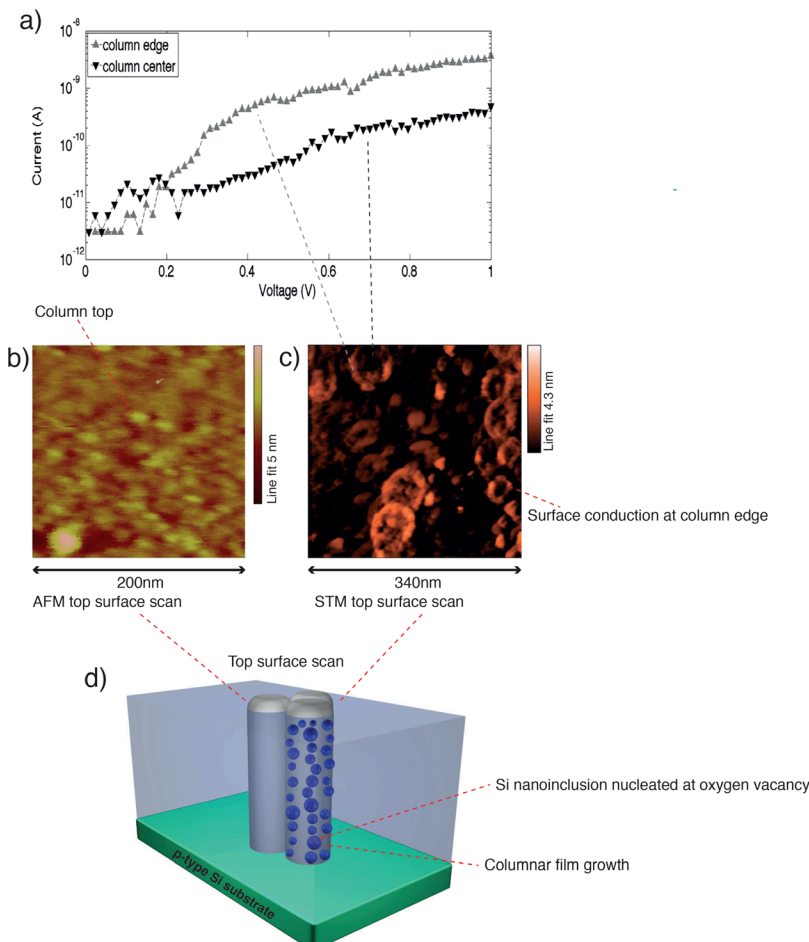


FIG. 6. (a) STM I/V curves for the edge point (b) atomic force microscopy scan of the surface top side showing surface features attributed to the tops of growth columns (c) Scanning tunneling microscopy scan of a sample surface [different area to that in (b)] showing enhanced conductivity at column edges (d) Schematic of columnar structure of switching film and switchable site.

initial stages of annealing, subnanometer clusters nucleate at oxygen vacancies,²⁰ increasing in number and growing by Ostwald ripening at longer times and/or higher temperatures as silicon diffuses. We propose that voltages applied across our devices drive oxygen vacancy migration, producing a field-driven phase separation of the active layer.²¹ This separation is enhanced by structural defects such as nanoscale cracks or inclusions;¹⁸ significantly, films grown by sputtering typically exhibit columnar or granular growth;¹⁶ boundaries between adjacent growth columns constitute structural defects that can nucleate phase separation. The rate of nucleation, as well as the number density and size of silicon nano-inclusions produced by the migration of oxygen vacancies, will increase with applied field until a critical point at which percolation pathways can be formed along the column boundaries (corresponding to the “set” process). Current transport in devices in the ON state is by trap assisted tunneling, suggesting that conductive pathways through our material are not continuous filaments, but instead a sequence of separate but neighboring silicon nano-inclusions (analogous to aggregated oxygen vacancies). The low activation energy in ON state (found for the TAT fit) is typical for conduction through oxygen vacancy defects. Such a low value is understandable if we assume that transport is through a semi-continuous array of adjacent silicon nano-inclusions in a sub-oxide matrix. The stoichiometry of the interinclusion matrix varies with applied field and Joule heating, with a more stoichiometric matrix (in the case of a partially OFF device) yielding a higher barrier height than for a very Si-rich matrix. The proposed process is shown schematically in Fig. 7.

The switching process is intrinsically unipolar [Fig. 2(a)], though we employ bipolar operation as this enables

more stable programming [unipolar programming is shown for illustrative purposes in Fig. 2(b)]. We note that full unipolar switching has not been seen for all devices studied. We relate this with the position of a weak (switching) point. Rather than the conductive filament being semi-continuous through the film, we suppose that there is a region located close to the top or bottom of the film that is depleted of silicon nano-inclusions. Such a structure has been reported in metal oxide films containing conductive nanofilaments in which the initial electroforming step generates an excess of vacancies close to the anode.²² As a result, a highly resistive region forms close to the cathode. As shown in Fig. 8, two configurations of the high resistance state are possible in this case, dependent on the polarity of the electroforming step. Configuration 1 shows a switching point near the ITO/*n*-type poly silicon — SiO_x interface; configuration 2 shows it near the SiO_x — substrate interface. Arrows show the movement direction of oxygen ions under the applied field. In the first configuration the set process occurs more easily in the negative bias as oxygen ions move downward and oxygen vacancies (silicon nano-inclusions) are left in the insulating (switching) gap making it more conductive. Similarly, for the second configuration the positive bias will more effectively initiate the set process. It is known that the silicon/silica interface is more favorable for the formation of oxygen vacancies²³ and thus more porous — consequently, in our system the second configuration is more plausible.

We note that previous reports of resistive switching in SiO_x have proposed a redox process,²³ though at the time little direct supporting evidence was available. However, it is well known that oxygen vacancies can be highly mobile

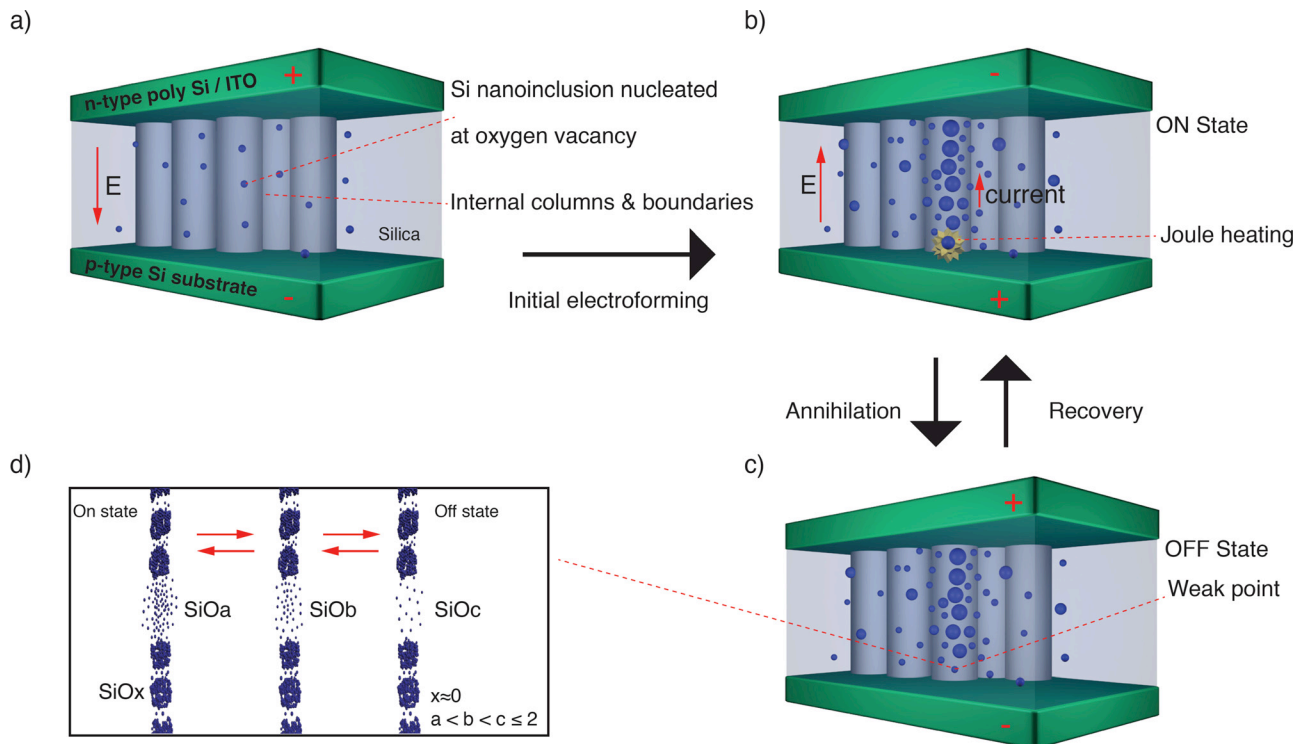


FIG. 7. Schematic of one cycle process. (a) Initial OFF state before applying the electric field, showing as-grown silicon nano-inclusions nucleated at oxygen vacancy sites. (b) ON state after the chain formation, showing extra silicon nano-inclusions produced by field-driven migration of oxygen vacancies. (c) Annihilation process due to Joule heating. (d) Silicon and oxygen distribution at the weak point.

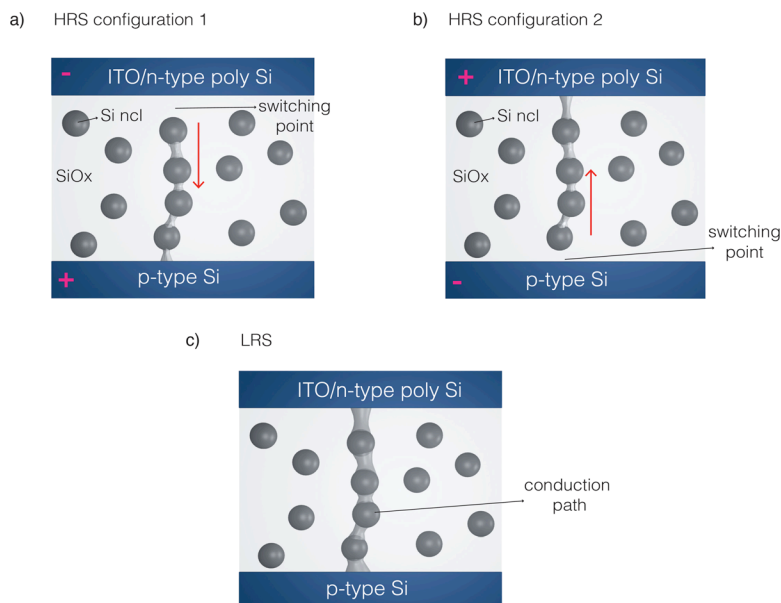


FIG. 8. Different positions of switching point due to depletion of oxygen vacancies close to one interface (a) high resistive state: switching point near ITO/ poly-Si-SiO_x interface; (b) high resistive state: switching point near SiO_x - substrate interface; (c) low resistive state.

in oxide matrices,²² and recent detailed work on resistive switching in metal oxides proposes a key role for oxygen vacancies in the formation of conductive filaments. Moreover, very recent TEM studies, published by the authors of Ref. 4 since the original submission of our manuscript, show the formation of conductive filaments at the surface of SiO_x by field-driven structural transitions in SiO_x resulting in discontinuous filaments composed of silicon nanoclusters and nanocrystals.²⁴ This supports our proposed mechanism.

Although Joule heating is the main driving force for the reset process, the electric field undoubtedly plays an important role. It is known that the silicon/silica interface is more favorable for the formation of oxygen vacancies²⁵ and thus more porous. Consequently, it is more likely that the position of the weak (switching) point is near the substrate/silica interface. As the oxygen vacancies behave as positively charged species, vacancies would be pushed toward the substrate during the set process (positive bias), recovering the broken path. In the reset process (negative bias) energy from the high local Joule heating overcomes the binding energy of vacancies, and the electric field consequently pushes them toward the top electrode, rapturing the conduction path.

IV. CONCLUSION

In conclusion, we report a study of resistive switching in silicon-rich silicon dioxide films grown by co-sputtering. Our results suggest that conductive pathways are formed at grain boundaries by the field-driven nucleation of oxygen vacancies. Such pathways are not continuous, but are chains of silicon nanoinclusions separated by a highly substoichiometric oxide matrix. A combination of applied field and Joule heating controls the distribution of oxygen vacancies, which is reflected in changes in the device resistance of four orders of magnitude or more. Our memristive RRAM device differs from those previously reported by not requiring diffusing metallic contacts,⁵ and not being limited by surface

conduction to vacuum operation.⁴ The resistive states are stable, switching pulses can be 90 ns or shorter, and switching currents are around 10 μ A. Such devices are very promising for application in memristive systems such as high-density semiconductor memories. We note that further investigation (underway) should yield more detailed insight into the microscopic switching mechanism.

ACKNOWLEDGMENTS

We acknowledge the valuable assistance provided by Steve Etienne (cleanroom processing). AM was supported by a UCL Overseas Research Scholarship. Funding was provided by EPSRC.

¹P. Heremans, G. H. Gelinck, R. Muller, K. J. Baeg, D. Y. Kim, and Y. Y. Noh, *Chem. Mater.* **23**(3), 341–358 (2011).

²L. O. Chua, *IEEE Trans. Circuit Theory* **CT18**(5), 507–519 (1971).

³D. B. Strukov, G. S. Snider, D. R. Stewart, and R. S. Williams, *Nature* **443**(7191), 80–83 (2008).

⁴J. Yao, Z. Z. Sun, L. Zhong, D. Natelson, and J. M. Tour, *Nano Lett.* **10**(10), 4105–4110 (2010).

⁵S. H. Jo, K. H. Kim, and W. Lu, *Nano Lett.* **9**(1), 496–500 (2009).

⁶A. Sinitskii and J. M. Tour, *ACS Nano* **3**(9), 2760–2766 (2009).

⁷M.-J. Lee, C. B. Lee, D. Lee, S. R. Lee, M. Chang, J. H. Hur, Y.-B. Kim, C.-J. Kim, D. H. Seo, S. Seo, U.-I. Chung, I.-K. Yoo, and K. Kim, *Nature Mater.* **01**(8), 625–630 (2011).

⁸S. H. Jo and W. Lu, *Nano Lett.* **8**(2), 392–397 (2008).

⁹R. Huang, L. J. Zhang, D. J. Gao, Y. Pan, S. Q. Qin, P. R. Tang, Y. M. Cai, and Y. Y. Wang, *Appl. Phys. A* **102**(4), 927–931 (2011).

¹⁰C. M. Liu, W. L. Liu, W. J. Chen, S. H. Hsieh, T. K. Tsai, and L. C. Yang, *J. Electrochem. Soc.* **152**(3), G234–G239 (2005).

¹¹F. El Kamel, P. Gonon, C. Vallee, V. Jousseume, and H. Grampeix, *Appl. Phys. Lett.* **98**(2), 023504 (2011).

¹²E. Barsoukov, MacDonald, J. Ross, *Impedance Spectroscopy: Theory, Experiment, and Applications* (Wiley, Hoboken, New Jersey, 2005).

¹³D. J. Dimaria, D. W. Dong, C. Falcony, T. N. Theis, J. R. Kirtley, J. C. Tsang, D. R. Young, F. L. Pesavento, and S. D. Brorson, *J. Appl. Phys.* **54**(10), 5801–5827 (1983).

¹⁴M. Porti, M. Avidano, M. Nafria, X. Aymerich, J. Carreras, and B. Garrido, *J. Appl. Phys.* **98**(5), 056101 (2005).

¹⁵O. Jambois, Y. Berencen, K. Hijazi, M. Wojdak, A. J. Kenyon, F. Gourbilleau, R. Rizk, and B. Garrido, *J. Appl. Phys.* **106**(6), 063526 (2009).

- ¹⁶M. T. P. McCann, D. A. Mooney, M. Rahman, D. P. Dowling, and J. M. D. MacElroy, *ACS Appl. Mater. Interfaces* **3**(2), 252–260 (2011).
- ¹⁷L. A. Nesbit, *Appl. Phys. Lett.* **46**(1), 38–40 (1985).
- ¹⁸G. A. Kachurin, K. S. Zhuravlev, N. A. Pazdnikov, A. F. Leier, I. E. Tyschenko, V. A. Volodin, W. Skorupa, and R. A. Yankov, *Nucl. Instrum. Methods Phys. Res. Sec. B* **127**, 583–586 (1997).
- ¹⁹S. Cuff, C. Labbe, B. Dierre, F. Fabbri, T. Sekiguchi, X. Portier, and R. Rizk, *J. Appl. Phys.* **108**(11), 113504 (2010).
- ²⁰C. R. Mokry, P. J. Simpson, and A. P. Knights, *J. Appl. Phys.* **105**(11), 114301 (2009).
- ²¹A. Sarikov, V. Litovchenko, I. Lisovskyy, I. Maidanchuk, and S. Zlobin, *Appl. Phys. Lett.* **91**(13), 133109 (2007).
- ²²G. Bersuker, D. C. Gilmer, D. Veksler, P. Kirsch, L. Vandelli, A. Padovani, L. Larcher, K. McKenna, A. Shluger, V. Iglesias, M. Porti, and M. Nafria, *J. Appl. Phys.* **110**, 124518 (2011).
- ²³J. Yao, L. Zhong, D. Natelson, and J. M. Tour, *Appl. Phys. A* **102**(4), 835–839 (2011).
- ²⁴J. Yao, L. Zhong, D. Natelson, and J. M. Tour, *Sci. Rep.* **2**, 242 (2012).
- ²⁵A. X. Chu and W. B. Fowler, *Phys. Rev. B* **41**(8), 5061–5066 (1990).